ESC European Society of Cardiology

Cardiovascular Research (2017) **113**, 1677–1687
doi:10.1093/cvr/cvx188

CXCL12-CXCR4 signalling plays an essential role in proper patterning of aortic arch and pulmonary arteries

Bo-Gyeong Kim[1], Yong Hwan Kim[2], Edward L. Stanley[3], Eva M. Garrido-Martin[2], Young Jae Lee[1]*, and S. Paul Oh[1,2]*†

[1]Lee Gil Ya Cancer and Diabetes Institute, Gachon University, 155 Gaetbeol-ro, Yeonsu-gu, Incheon 21999, Republic of Korea; [2]Department of Physiology and Functional Genomics, College of Medicine, University of Florida, 1600 SW Archer Road, Room CG-20B, Gainesville, FL 32610, USA; and [3]Department of Herpetology, Florida Museum of Natural History, University of Florida, Gainesville, FL 32610, USA

Received 30 November 2016; revised 27 June 2017; editorial decision 16 August 2017; accepted 8 September 2017; online publish-ahead-of-print 11 September 2017

Time for primary review: 56 days

Aims Chemokine CXCL12 (stromal derived factor 1: SDF1) has been shown to play important roles in various processes of cardiovascular development. In recent avian studies, CXCL12 signalling has been implicated in guidance of cardiac neural crest cells for their participation in the development of outflow tract and cardiac septum. The goal of this study is to investigate the extent to which CXCL12 signalling contribute to the development of aortic arch and pulmonary arteries in mammals.

Methods and results Novel *Cxcl12*-LacZ reporter and conditional alleles were generated. Using whole mount X-gal staining with the reporter allele and vascular casting techniques, we show that the domain branching pattern of pulmonary arteries in *Cxcl12*-null mice is completely disrupted and discordant with that of pulmonary veins and airways. *Cxcl12*-null mice also displayed abnormal and superfluous arterial branches from the aortic arch. The early steps of pharyngeal arch remodelling in *Cxcl12*-null mice appeared to be unaffected, but vertebral arteries were often missing and prominent aberrant arteries were present parallel to carotid arteries or trachea, similar to aberrant vertebral artery or thyroid ima artery, respectively. Analysis with computed tomography not only confirmed the results from vascular casting studies but also identified abnormal systemic arterial supply to lungs in the *Cxcl12*-null mice. *Tie2*-Cre mediated *Cxcr4* deletion phenocopied the *Cxcl12*-null phenotypes, indicating that CXCR4 is the primary receptor for arterial patterning, whereas *Cxcl12* or *Cxcr4* deletion by *Wnt1*-Cre did not affect aortic arch patterning.

Conclusion CXCL12-CXCR4 signalling is essential for the correct patterning of aortic arches and pulmonary arteries during development. Superfluous arteries in *Cxcl12*-null lungs and the aortic arch infer a role of CXCL12 in protecting arteries from uncontrolled sprouting during development of the arterial system.

Keywords CXCL12 • CXCR4 • Aortic arch anomaly • Pulmonary artery patterning • Vertebral artery • Cardiac neural crest

1. Introduction

CXCL12, also called stromal derived factor 1 (SDF1), is a pleiotropic chemoattractant factor involved in B cell lymphopoiesis, homing of bone marrow stem cells, and cardiovascular development.[1–3] The function of CXCL12 signalling is mediated by two chemokine receptors, CXCR4, and CXCR7.[2,4] Studies for the developmental role of the CXCL12-CXCR4 axis using animal models have shown that it is involved in various cardiovascular developmental processes, including vascular repair, alignment of arterial vessels with peripheral nerves, and development of mesenteric arteries, coronary arteries, the outflow tract and the ventricular septum.[5–9] However, the role of CXCL12 in the development of the aortic arch and pulmonary arteries has yet to be fully explored.

* Corresponding authors. Tel: +82 32 899 6590; fax: +82 32 899 6039, E-mail: leeyj@gachon.ac.kr (Y.J.L.); Tel: 352 273 8232; fax: 352 846 2700, E-mail: ohp@ufl.edu (S.P.O.)

†Present address. Department of Neurobiology, Barrow Neurological Institute/ Dignity Health, St Joseph's Hospital and Medical Center, 350 W. Thomas Rd, Phoenix, AZ 85012, USA; Tel: +1 602 406 3732; fax: +1 602 406 4172, E-mail: ohp@barrowneuro.org

Aortic arch development requires precise stepwise remodelling of five pairs of pharyngeal arch arteries in mammals, involving sprouting/splitting, elongation, and regression.[10–12] Numerous variations of congenital cardiac outflow tract and aortic arch anomalies such as DiGeorge syndrome have been reported in humans.[13] Studies with genetically engineered mouse models recapitulated most of these anomalies, including the persistent truncus arteriosus, double aortic arch, right-sided aortic arch, interruption of the aortic arch, aberrant origin of the right subclavian artery, and lack of the common carotid arteries.[10,11] A subset of neural crest cells (NCCs), termed cardiac NCCs contribute to proper septation of the outflow tracts, and the development of cardiac valves, ventricular septum, and the pharyngeal arch arteries.[11] A large number of genes whose mutations give rise to defects in the outflow tract and the aortic arch have shown to be involved in the guidance, migration, and survival of NCCs.[10] CXCL12-CXCR4 signalling was shown to guide cardiac NCCs, and impaired CXCL12 signalling in cardiac NCCs led to outflow tract defects and ventricular septal defects in an avian study.[14] Recently, CXCL12 and CXCR4 have been implicated in DiGeorge syndrome as downstream effectors of TBX1 for pharyngeal NC development.[15,16] However, the role of CXCL12 signalling in cardiac NCC guidance in mammals remains to be investigated.

Pulmonary circulation must be coordinated with airway passages for efficient oxygen exchange. Compared to the aortic arch patterning, little is known about pulmonary artery patterning. While the mechanisms and genes involved in airway branch patterning have been uncovered,[17,18] those involved in pulmonary artery patterning have been scarcely reported to date. Since the airway passages and pulmonary arteries need to be closely associated, it is conceivable that some chemoattractant factors like CXCL12 from the airway may guide the branching of pulmonary arteries.

In the present study, we utilized novel *Cxcl12*-lacZ reporter, -null, and -conditional knockout mice to study expression and function of CXCL12 in cardiovascular development. We show here that CXCL12-CXCR4 paracrine signalling is essential for the proper branch patterning of aortic arch and pulmonary arteries.

2. Methods

2.1 Animals

Cxcl12-conditional knockout (cKO) mouse strains were generated at Gachon University. *β-actin*-Cre, ROSA26^{FLPe}, *Tie2*-Cre, *Tagln*-Cre, *Nkx2.1*-Cre, *Wnt1*-Cre, and *Cxcr4*-cKO were purchased from Jackson laboratory, and *Shh*-Cre was provided by B. Harfe (University of Florida). All mice have been maintained under standard specific-pathogen-free (SPF) conditions and all animal procedures were reviewed and approved by the Institutional Animal Care and Use Committee of Gachon University (LCDI-2012-0024; LCDI-2015-0046) and the University of Florida (UF 201405611; UF 201401417). All animal procedures conformed to the NIH guidelines (Guide for the care and use of laboratory animals). Mice were on a mixed genetic background of C57BL/6J and 129SvJ.

2.2 Construction of conditional knock-out vector for targeting Cxcl12

A BAC clone (129S7/AB2.2 library, bMQ-226c10) containing mouse *Cxcl12* gene was obtained from Sanger Institute Resources (Geneservice, UK). A *Cxcl12*-targeting vector was constructed using a recombineering system [https://ncifrederick.cancer.gov/research/brb/recombineeringInformation.aspx (15 September 2017, date last accessed)]. A 10.6-kb genomic DNA fragment of *Cxcl12* was retrieved from the BAC DNA and inserted into pLMJ235 possessing the herpes simplex virus thymidine kinase (HSV-TK) gene as a negative selection marker. An frt-SD/SA-IRES-LacZ-Neo-frt-loxP (LacZ/Neo) cassette including a reporter (LacZ) and a positive selection marker (Neo, neomycin-resistant gene) was inserted 923-bp downstream of exon 2. A loxP sequence was cloned 278-bp upstream of exon 2.

2.3 Generation for Cxcl12 conditional knock-out mice

The targeting vector was linearized with NotI and electroporated into 2 x 10^7 J1 ES cells. Approximately 300 G418 and 1-(2-deoxy-2-fluoro-1-β-D-arabinofuranosyl)-5-iodouracil (FIAU)-resistant colonies were randomly picked. Homologous recombination was screened by genomic Southern blot analyses using external 5' and 3' probes. Targeted ES cells were injected into blastocysts of the C57BL/6 (B6) strain. ES cell culture and blastocyst injections were performed by standard methods. Chimeric male mice were mated with B6 females to establish the *Cxcl12*^{lacZ} (*Cxcl12*^{3f}) strain on a 129/B6 hybrid background. Germ-line transmission of the targeted allele was confirmed by Sothern blot analyses. *Cxcl12*$^{+/3f}$ mice were crossed with FLP–deleter mice (ROSA26FLPe)[19] to remove the LacZ/Neo cassette flanked by the frt sequences for generating the conditional *Cxcl12*$^{+/2loxP(2f)}$ mice. *Cxcl12*$^{+/3f}$ mice were also crossed with *β-actin*-Cre[20] to generate the *Cxcl12*$^{+/1loxP(1f)}$ allele in which the LacZ/Neo cassette and exon 2 were deleted. Genotypes of wild-type, 3f, 2f, and 1f *Cxcl12* alleles were analysed by PCR using the primer sets listed in Supplementary material online, *Table S1*.

2.4 X-gal staining, histology, immunohistochemistry, and whole mount *in situ* hybridization

Whole mount X-gal staining was performed as previously described.[21] For the whole-mount imaging, samples were sequentially dehydrated using increasing concentration of methanol, cleared with an organic solvent (benzyl alcohol: benzyl benzoate = 1: 1; Sigma), and photographed under a stereo dissection microscope. For the histological analysis, X-gal stained samples were embedded in paraffin following hydration and clearing. 5 to 7-μm thick sections were counterstained with nuclear fast red (NFR, Vector laboratories), or were immunostatined with mouse monoclonal antibodies against α-smooth muscle actin (SMA; clone: 1A4; Sigma, A5228), and rabbit polyclonal antibodies against von Willebrand Factor (vWF; 1: 200; Dakocytomation, A0082, Denmark). The secondary antibody reactions and color development were carried out with the Vector M.O.M staining kit (Vector Laboratories) for SMA, and a Polink-1 AP Rabbit with Permanent Red kit (GBI Labs) for vWF, according to the manufacturers' instructions.

2.5 Latex dye injection

Pregnant mice were euthanized by decapitation following anesthesia with isoflurane. Embryos at a late gestational period (E16.5–E18.5) and neonates were anesthetized by placing them on ice. Abdominal and thoracic cavities were opened. For perfusion through pulmonary arteries, blue latex dye (Connecticut Valley Supply Co) was slowly and steadily injected into the right ventricle using a mouth capillary pipet with elongated glass capillary tubes. For visualizing pulmonary venous

network, yellow dyes were injected by advancing the capillary tube to the left atrium through the left ventricle. For the airway, yellow dye was injected from the trachea. Injected samples were briefly washed in PBS and fixed overnight in formalin. For visualizing vasculature of early stage embryos (E9.5–E15.5), diluted latex dye was used. For acquiring perfusion images of the lungs, the heart and lungs were isolated, dehydrated with methanol, and cleared with organic solvents (benzyl alcohol and benzyl benzoate 1: 1, Sigma) prior to photography.

2.6 Quantification of air saccule area of the embryonic lungs

Pregnant mice were euthanized as described above. The body weights of E14.5 and E17.5 embryos were measured. Lungs were weighed after removal of the hearts. Air saccule area of the left lungs was measured from H&E stained sections using the NIH Image J software. Four non-overlapping fields (x100 magnification at E14.5 and x40 magnification at E17.5) of each embryonic lung section were analysed ($n = 5$ per each stage and genotype).

2.7 *In situ* hybridization of *Isl1*

X-gal stained embryos were fixed in 10% formalin for 16 h at RT, and were embedded in paraffin. *Isl1* probe (NM_021459.4, 145-1437 bp, Cat No. 451931) and RNAscope 2.5HD reagent kit-Brown (Cat No. ACD-322300) were purchased from Advanced Cell Diagnostics (ACD, USA). All experimental steps followed the manufacturer's protocol. The sections were incubated in 100% ethanol for 2 min twice, and dried for 5 min at RT. RNAscope hydrogen peroxide was applied on each section for 10 min at RT and washed in water 2 times. The sections were submerged into boiling 1X Target Retrieval solution for 15 min, washed with water and 100% ethanol, and air dry. Each section was treated with protease for 30 min at RT, washed with water then added several drops of *Isl-1* probe for 2 h at 40 °C. After the sections were washed with 1X washing buffer, Amp reagents (Amp1-6, for amplifying signals) were applied on each section for 30 min (Amp1, 3, at 40 °C; Amp5, at RT) or 15 min (Amp2, 4, at 40 °C; Amp6, at RT). Every amplifying step, the sections were washed with 1X washing buffer. To detect the signal, BROWN-A and BROWN-B reagents were mixed equal volume and added each section for 10 min at RT. The slides were washed in water and dehydrated with 70% and 100% ethanol, incubated in 100% Histo-H3 xylene substrate for 5 min. The slides were mounted and photographed under microscope.

2.8 Diffusible iodine contrast enhanced computed tomography (diceCT)

E17.5 WT and mutant embryos were fixed in 10% buffered formalin for 2–3 days at room temperature, and were soaked Lugol's Iodine (1.25% iodine and 2.5% potassium iodine: Carolina Biological Supply) for 5–7 days. The samples were scanned in a Phoenix v|tome|x M scanner (GE's Measurement & Control business) using a 180 kV X-ray tube with a tungsten-coated diamond target, under the following settings: Current = 110 mA, Voltage = 100 kV, detector capture time = 0.333 s, three image averaging. The resulting 2 D X-ray data were processed using GE's proprietary datos|x software v 2.3 to produce a series of tomograms. These image stacks were then compiled and the various components of the circulatory and pulmonary system sectioned out, measured, and analysed using VG StudioMax 3.0 (Volume Graphics).

2.9 Quantitative real-time RT-PCR analysis

Total RNA was isolated using a NucleoSpin RNA II kit (BD Biosciences) following the manufacturer's protocol. Samples were treated with DNase I from the kit to remove contaminating DNA. For cDNA synthesis, 2 μg of total RNA for each sample was reverse transcribed using a PrimeScript RT Master Mix (TAKARA). The reaction was carried out at 37 °C for 15 min and 85 °C for 5 s. For RT-PCR, the PCR reaction mixture and hot-start PCR reaction were performed. For the amplification of RNAs for *Cxcl12* and *GAPDH*, a total of 25 cycles were run. The primers used for RT-PCR are summarized in Supplementary material online, *Table S2*. Quantitative RT-PCR was performed using SYBR Premix DimerEraser Kit (TAKARA) and a CFX384 Real-Time PCR Detection System (Bio-rad). Each reaction contained 10 μL of master mix solution, 0.3 μM concentration of each primer, and 3.8 μL of template cDNA. RNase-free water was added to a total volume of 20 μL. Amplification was performed in triplicate using the mouse cyclophilin (mCyclo) gene as a control. Denaturation at 95 °C for 10 min was followed by 39 cycles of denaturation at 95 °C for 15 s, annealing at 60 °C for 1 min, and 1 cycle of denaturation at 95 °C for 15 s, annealing at 60 °C for 15 s, and 95 °C for 0.5 s. The change in fluorescence SYBR Green in every cycle was monitored by the CFX384 Real-Time PCR Detection System. A mouse Cyclophilin primer set was used to normalize the amount of total cDNA in each sample. Predesigned PCR primer sets for *Cxcl12* (PrimerBank ID 7305465a1) were used to determine the amount of each cDNA in control and mutant samples. Each sample was run in triplicate. After 40 cycles of PCR reaction, the relative amount of each transcript was determined using the ΔΔCt method. Primer sequences for Quantitative real-time PCR are shown in Supplementary material online, *Table S2*.

2.10 Statistics

One-way ANOVA followed by Tukey's multiple comparison test and two-tailed Student's *t*-test were performed for statistical analyses using GraphPad Prism version 7.03 for Windows (GraphPad Software). Differences were considered significant when $P < 0.05$.

3. Results

3.1 *Cxcl12*^{3f} allele is a null allele

In order to systemically examine *Cxcl12* expression during embryonic development and adult stages, and to investigate the cell-type specific role of CXCL12, we generated reporter (*Cxcl12*^{LacZ}) and conditional (*Cxcl12*^{2f}) alleles of *Cxcl12* (*Figure 1*). Viable homozygous mice for the *Cxcl12*^{LacZ} (*Cxcl12*^{3f}) allele were undetectable at the weaning stage (see Supplementary material online, *Table S3*), indicating that *Cxcl12*^{3f} is a null or hypomorphic allele. Some *Cxcl12*$^{3f/3f}$ mice were found dead at late gestational period (E15-E18.5) or shortly after birth (see Supplementary material online, *Table S4*) similar to *Cxcl12*$^{1f/1f}$ mice (see Supplementary material online, *Table S5*), indicating that *Cxcl12*^{3f} is likely a null allele (*Cxcl12*^{1f}). Consistent with this finding, no *Cxcl12* transcript was detected in E17.5 *Cxcl12*$^{3f/3f}$ lungs as well as *Cxcl12*$^{1f/1f}$ lungs (*Figure 1F* and *G*). The most consistent and distinguishable morphological feature of *Cxcl12*$^{1f/1f}$ or *Cxcl12*$^{3f/3f}$ foetuses ($n > 60$) from their control littermates was a diverse range of tail defects (see Supplementary material online, *Figure S1*): haemorrhagic (see Supplementary material online, *Figure S1B* and *C*), curly or short (see Supplementary material online, *Figure S1D*),

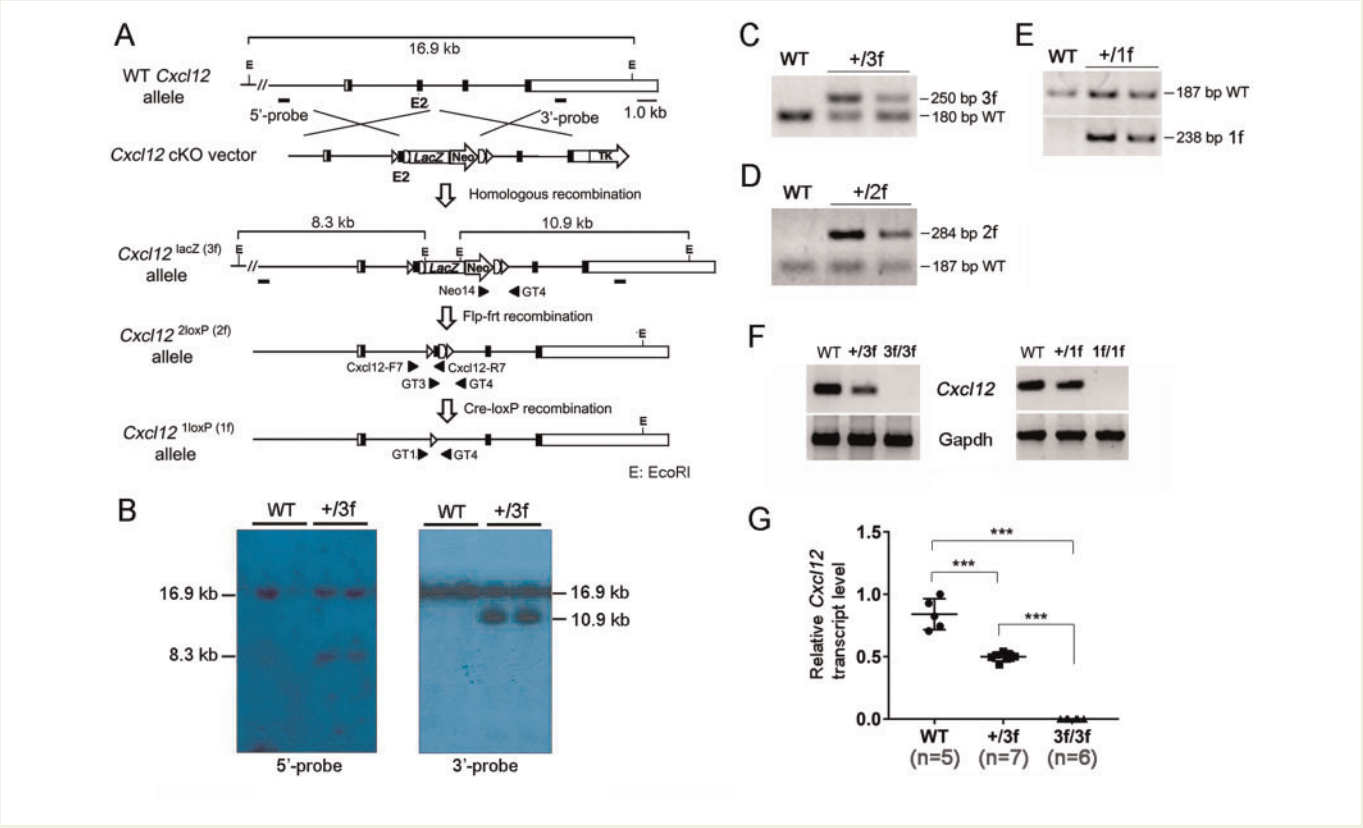

Figure 1 Generation of *Cxcl12* reporter and conditional allele. (*A*) Schematic diagram of the *Cxcl12* wild-type (WT), reporter ($Cxcl12^{lacZ(3f)}$), conditional ($Cxcl12^{2loxP(2f)}$), and null ($Cxcl12^{1loxP(1f)}$) alleles. The targeting vector consists of a 6, 763 bp 5'-homology arm, a 4, 626 bp 3'-homology arm, a LacZ/Neo cassette (SIBN: SA, splice donor and acceptor; IRES, internal ribosome entry sequence; LacZ, β-galactosidase gene; Neo, neomycin resistance gene) and a TK (herpes simplex virus thymidine kinase gene) cassette. Exons are represented by boxes. Coding region is indicated by black boxes. Frt sequences flanking the LacZ/Neo cassette and loxP sequences flanking exon2 are indicated by semicircles and triangles, respectively. The probes (5'-probe and 3'-probe) for Southern hybridization are shown in the WT alleles. Locations of primer pairs used for genotyping are indicated by arrowheads. E, EcoRI. (*B*) Southern blot analyses of mouse tail genomic DNA. Genomic DNA isolated from tails was digested with EcoRI and then hybridized with 5'-probe (left) and 3'-probe (right). Both probes detected a 16.9-kb fragment for the *Cxcl12* WT allele. For the $Cxcl12^{3f}$ allele, the 5'-probe and 3'-probe detected an 8.3 and 10.9 kb fragment, respectively. (*C–E*) Genotyping of heterozygous alleles of 3f (*C*), 2f (*D*), and 1f (*E*) with specific primer pairs: Neo14/GT4, GT3/GT4, and GT1/GT4, respectively. F and G. Semi quantitative (*F*) and quantitative (*G*) RT-PCR using a primer set from exon2 show the absence of *Cxcl12* transcripts in the lungs of E17.5 $Cxcl12^{3f/3f}$ (left panel in F and G) and $Cxcl12^{1f/1f}$ (right panel in F) foetuses. One-way ANOVA followed by Tukey's multiple comparison test was performed for statistical analysis. *** $P < 0.0001$.

edemic (see Supplementary material online, *Figure S1F–H*) tails. Most of $Cxcl12^{1f/1f}$ or $Cxcl12^{3f/3f}$ mutants had ventricular septal defects, consistent with previous reports[5] (data not shown).

3.2 Cxcl12 is mainly expressed in the cells composing arteries

Cxcl12 expression during development was examined by X-gal staining at various stages of $Cxcl12^{+/3f}$ and $Cxcl12^{3f/3f}$ embryos. At E10.5-12.5, X-gal-positive areas were found in the vasculatures alongside the spinal column (see Supplementary material online, *Figures S2A and B*). They were not found in developing heart *per se*, but in the systemic and pulmonary arteries (*Figures 2A–B*). Histological sections revealed that the X-gal-positive cells in the aorta are mainly adventitial cells (*Figures 2C–D*). The second heart field and neural crest cells are the main progenitor populations contributing to the developing outflow tract and pharyngeal arch arteries. X-gal-positive cells in the outflow tract were partially overlapped with Islet1 (Isl1)-expressing cells, which is a major marker of second heart field[22,23] (see Supplementary material online, *Figure S3*). In the pulmonary arteries, the X-gal-positive cells were found in all three layers of the arterial vessels: endothelial, smooth muscle, and adventitial cells (*Figures 2E–G*). *Cxcl12* expression in developing pulmonary arteries (PA) was first detected in major PA branches at E14.5 (*Figure 2H*), spread into smaller arterial branches in late gestational and newborn foetuses (*Figures 2I* and *J*), and faded away in the lungs of weaning stage mice (*Figure 2K*).

3.3 *Cxcl12*-depletion leads to disruption of domain branching patterns of pulmonary arteries

Interestingly, the X-gal stained PA branching pattern in $Cxcl12^{3f/3f}$ (*Figure 3B*) was clearly distinguishable from that in $Cxcl12^{+/3f}$ mice (*Figure 3A*). The second and third branches of normal pulmonary arteries follow the domain branching pattern: smaller size branches sprouting off from the main stalk parallel to one another (*Figure 3A* and see Supplementary

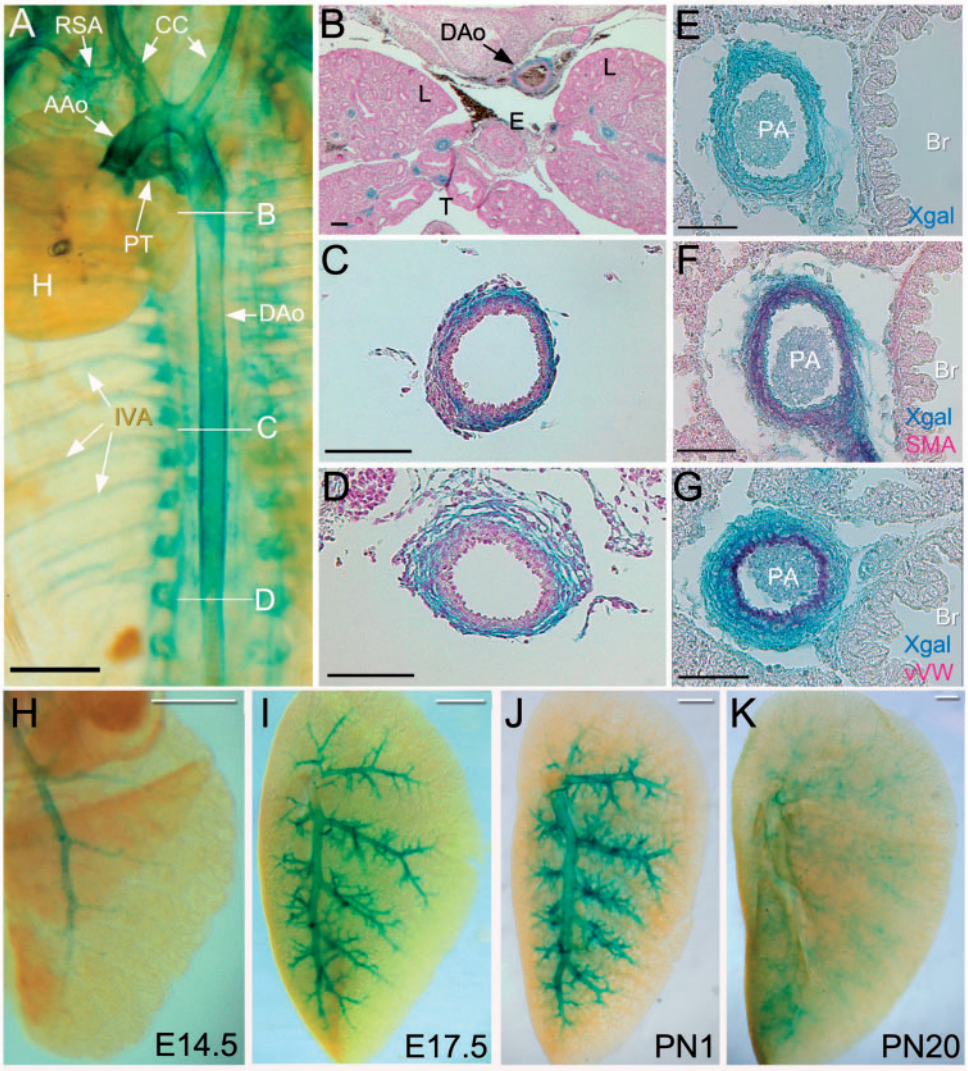

Figure 2 *Cxcl12* is expressed in systemic and pulmonary arteries: (*A*) Whole mount X-gal staining of *Cxcl12*$^{+/3f}$ embryos at E15.5. Internal organs except for the heart were removed. AAo, ascending aorta; CC, common carotid arteries; DAo, descending aorta; H, heart; IVA, intervertebral arteries; PT, pulmonary trunk; RSA, right subclavian artery. (*B–D*) Histological sections with x-gal staining show that Cxcl12 is expressed in the upper (*B*), middle (*C*), and bottom (*D*) of the descending aorta. L, lungs; E, oesophagus; T, trachea. Scale bars: A, 1 mm B, 200 μm C-D, 100 μm. (*E–G*) *Cxcl12* expression is detected in endothelial cells, smooth muscle cells and adventitial cells of pulmonary arteries. X-gal stained lung sections were stained with anti-αSMA (*F*) and Von Villebrand factor (vWF, *G*) antibodies. X-gal positive cells (blue) overlap with smooth muscle cells (*E*) and endothelial cells (*G*) of pulmonary arteries. Br, bronchus. PA, pulmonary artery. E-F, 50 μm. (*H–K*) Whole mount X-gal staining of the left lungs at various stages of *Cxcl12*$^{+/3f}$ mice. Scale bars: A-D, 500 μm.

material online, *Figure S4A*). The arterial branches of *Cxcl12*$^{3f/3f}$ mice deviate from this normal branching pattern: the primary branching point of pulmonary arteries occurs at a more proximal region than normal, and similar-sized multiple branches split off from the main branches (*Figure 3B* and see Supplementary material online, *Figure S4B*). Disruption of the PA branching pattern in *Cxcl12*$^{1f/1f}$ was confirmed by latex dye injection through the right ventricle (*Figures 3C* and *D*). In contrast, pulmonary venous and bronchial branching appeared to be largely unaffected (*Figures 3E–H*). The branching points of the PA were well aligned with those of bronchi in control mice (*Figure 3G*), but discordant in *Cxcl12*-null mice (*Figure 3H*). PAs branched off at more proximal sites with increased numbers in *Cxcl12*-null mice compared with controls. Such an abnormal PA branching pattern was observed in the earlier stages of lung development (see Supplementary material online, *Figure S5*). It is noteworthy that growth and maturation of airway sacculation were retarded in *Cxcl12*-null mice (see Supplementary material online, *Figure S6*). These results demonstrate that CXCL12 is essential for the proper branching of pulmonary arteries in alignment with airways and veins.

3.4 *Cxcl12*-depletion leads to abnormal aortic arch branching

All *Cxcl12*-null mice ($n > 20$) exhibited a significantly distended pulmonary trunk (see Supplementary material online, Video files *S1* and *S2*)

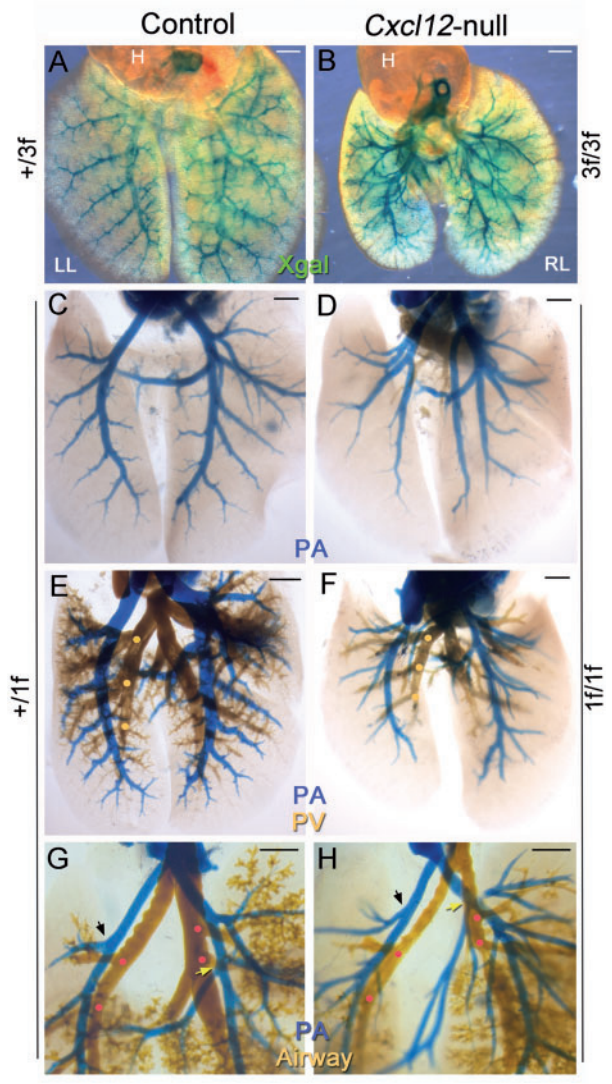

Figure 3 Abnormal pulmonary arterial branching patterns in *Cxcl12*-null mice. Each panel shows the dorsal view of E17.5 lungs (each panel, $n > 3$). (*A* and *B*) Whole mount X-gal staining of $Cxcl12^{+/3f}$ and $Cxcl12^{3f/3f}$ lungs and heart (H) demonstrates disruption of the domain branching pattern of pulmonary arteries in *Cxcl12*-mutants. Magnified images of left lung (LL) with tracing are shown in Supplementary material online, *Figure S3A* and *B*. (*C* and *D*) Pulmonary arteries (PA) visualized by blue latex dye injection via right ventricle also show abnormal arterial branching patterns in *Cxcl12*-null mice, consistent with the X-gal staining images shown in A and B. (*E* and *F*) PA and pulmonary vein (PV) are visualized by blue and yellow latex dyes, respectively. PV branching points (yellow dots) in the mutant (*F*) are comparable with that of control (*E*). PAs and PVs are regularly interspaced in the control lungs (*E*), whereas PA branches are uncoordinated with PV branches in the mutant (*F*). (*G* and *H*) PA and airways are visualized by blue and yellow latex dyes, respectively. The airway branching points (red dots) in the mutants (*H*) are largely unaffected. Arterial branching points are closely matched with bronchial branches (red dots) in the control mice, whereas in the mutants they are misaligned with the airway branches. The first arterial branches of the left lung (black arrows) and accessory lobe (yellow arrows) in the *Cxcl12*-mutants occur at more proximal sites than those in the controls. Scale bars: A–F, 1 mm; G–H, 500 μm.

and a diverse range of aberrant branching from the aortic arch (AA) in E17.5 *Cxcl12*-null mutants. The AA of normal mice gives rise to the brachiocephalic artery which divides into the right subclavian artery (RSA) and the right common carotid artery (RCC), left common carotid artery (LCC), and left subclavian artery (LSA) in the direction from the ascending to the descending aorta. The vertebral arteries (VAs) arise from the subclavian arteries, and elongate cranially to intersect with the basilar artery (*Figures 4A* and *A'*). The most noticeable features of AA in the *Cxcl12*-mutants are the presence of numerous superfluous arterial branches and a prominent artery in parallel to LCC or along the trachea (*Figures 4B–F*). We presume that this aberrant artery is the vertebral artery with aberrant origins,[24] since VAs were often absent from the subclavian arteries in the *Cxcl12*-mutants. In some cases, one or two arteries were found in the central location, resembling the thyroid ima arteries (TIA, *Figures 4B, D,* and *E*).[25] The LSA originates from the descending aorta at or just above the junction of the ductus arteriosus (DA) in control mice, but it branches off from the descending aorta below DA in *Cxcl12*-mutants (*Figure 4F*).

3.5 *Cxcl12*-depletion results in superfluous arterial branching and failure of formation of the vertebral arteries

For a better understanding of the AA anomaly in *Cxcl12*-mutants, we examined control and mutant embryos at earlier stages. At E13.5, the AA pattern of *Cxcl12*-mutants appeared to be similar with that of E17.5 shown in *Figure 4*. *Figure 5B* shows a representative example, having an extra artery originated from AA in parallel with a thin LCC in E13.5 *Cxcl12*-mutants. In control E12.5 embryos (*Figure 5C*), latex dye perfusion visualized the common carotid artery (CCA) extending from the third pharyngeal artery (A3), as well as the fourth (A4), and the sixth (A6) pharyngeal arteries which develop into the aortic arch and pulmonary trunk, respectively. The VAs were shown to connect subclavian arteries to the basilar artery (BA). Variable forms of abnormal arterial patterns were observed in E12.5 *Cxcl12*-mutants, but the most common and noticeable feature of *Cxcl12*-mutants was the absence of VAs and additional aberrant arterial branches (*Figure 5D*). In E11.5 embryos, abnormal superfluous arteries originated from AA were observed (*Figure 5F*). The development of three pairs of pharyngeal arch arteries (A3, A4, and A6) in E10.5 embryos are largely unaffected in *Cxcl12*-mutants (*Figure 5H*).

3.6 Diffusible iodine contrast-enhanced computed tomography (diceCT)

To validate the pulmonary artery and aortic arch phenotype of *Cxcl12*-null mice, we employed diceCT,[26,27] which utilizes diffusible iodine as a contrasting agent. This method allows the high-resolution visualization of all internal structures by diffusing x-ray iodine into the soft tissues of the specimen, thereby overcoming potential artefacts caused by injection of casting or contrasting agents, while allowing thorough examination of vascular network from three dimensional images. Five wild-type and six *Cxcl12*-mutants at E17.5 were used to collect the vascular images, scanned at resolutions of 11.0–11.9 μm. The CT images nicely recapitulate those obtained from latex-perfused lungs. Pulmonary arteries, veins, and airways are well-coordinated as they parallel to one another in control lungs (see Supplementary material online, *Figures S7A–D*). In the mutant lungs, however, pulmonary arteries appeared discordinated with the pulmonary vein and airways (see Supplementary material online, *Figures S7E–H*). The discordance of parallel alignment between PAs and

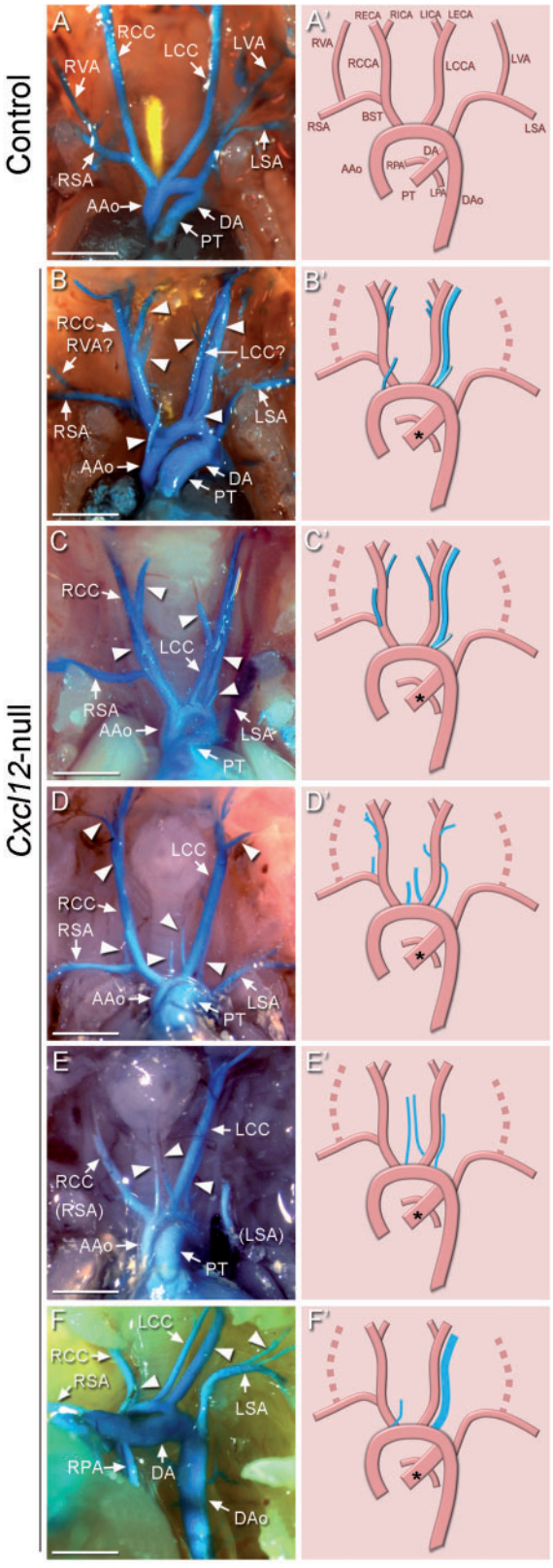

Figure 4 Abnormal branching patterns of aortic arches in *Cxcl12*-null mice. Blue latex dye-perfused images of the aortic arch arteries in control (*A*, $n > 5$) and *Cxcl12*-mutants (*B–F*, $n > 20$) at E17.5. Arrowheads indicate abnormal arterial branches. Two parallel arteries originating from the aortic arch were often found in *Cxcl12*-mutants (*B*, *C*, *F*). One of them should be the left common carotid artery, and the other is presumably an abnormal vertebral artery (marked with '?'). Right panels are diagrams corresponding to images of the vasculature shown in the left panels. Abnormal arteries were shown with the blue lines, and missing arteries are shown with dotted lines. The asterisks indicate distended pulmonary trunk. AAo: ascending aorta; BST: brachiocephalic trunk; DA: ductus arteriosus; DAo: descending aorta; LCCA and RCCA: left and right common carotid artery; LECA and RECA: left and right external carotid artery; LICA and RICA: left and right internal carotid artery; LPA and RPA: left and right pulmonary artery; LSA and RSA: left and right subclavian artery; LVA and RVA: left and right vertebral artery; PT: pulmonary trunk. Scale bars: A–F, 1 mm.

neighboring airways was measured by the angles between them (see Supplementary material online, *Figures S8A and F*): the angle was significantly wider in the mutants compared to that in controls (see Supplementary material online, *Figure S8E*). The diceCT 3D images for AA arteries were also consistent with the data from latex perfusion shown in *Figure 4*. The common features of six E17.5 mutants analysed by diceCT are the presence of an abnormal artery raised from the ascending aorta parallel to trachea, an abnormal artery from aortic arch parallel to LCC, numerous abnormal arterial branches from various areas of AA arteries, abnormally lowered position of left subclavian artery, and absence of clear vertebral arteries (*Figures 6B–E*). In addition to these phenotypes, we also found systemic arteries supplying to lungs in three of these mutants (*Figures 6B, D,* and *E*)

3.7 CXCR4 is the primary receptor of CXCL12 for arterial patterning

CXCL12 signals can be mediated by CXCR4 or CXCR7 receptors, both of which are expressed in multiple cell types including endothelial cells.[28–30] To delineate the signalling, we first deleted *Cxcr4* using *Tie2*-Cre. *Tie2*-Cre; $Cxcr4^{f/f}$ mice recapitulated *Cxcl12*-null phenotypes, including distended pulmonary trunk and superfluous aortic arch branching (*Figures 7A–C*), abnormal pulmonary artery branching patterns (*Figures 7D–F*), and tail defects (*Figures 7G and H*). Previously it was shown that *Cxcr7*-null and *Tie2*-Cre; $Cxcr7^{f/-}$ mice exhibited semilunar valve stenosis but not the phenotypes in AA or pulmonary artery defects.[30,31] This result clearly demonstrates that CXCR4 is the primary receptor for CXCL12 for proper arterial branching and patterning. In addition, the tail defects are associated with an abnormal vascular circuit resulting from impaired CXCL12 signal in *Tie2*-expressing cells via CXCR4. To investigate the extent to which CXCL12-CXCR4 signalling in NCCs is involved in AA patterning, we deleted *Cxcl12* or *Cxcr4* in NCCs using *Wnt1*-Cre mice. We were able to recover viable *Wnt1*-Cre; $Cxcl12^{2f/2f}$ ($n > 10$) and *Wnt1*-Cre; $Cxcr4^{f/f}$ mice ($n = 7$) in concordance with expected Mendelian ratios, and none of them showed defects in branching patterning of AA or pulmonary arteries.

4. Discussion

In the present study, we show that that CXCL12-CXCR4 paracrine signalling is essential for the proper branching patterning of aortic arch and pulmonary arteries.

In the developing limb skin model, peripheral nerves secrete CXCL12 which is crucial for the alignment of arterial vessels with peripheral nerves.[9] Interestingly, our studies show that *Cxcl12* is expressed in the

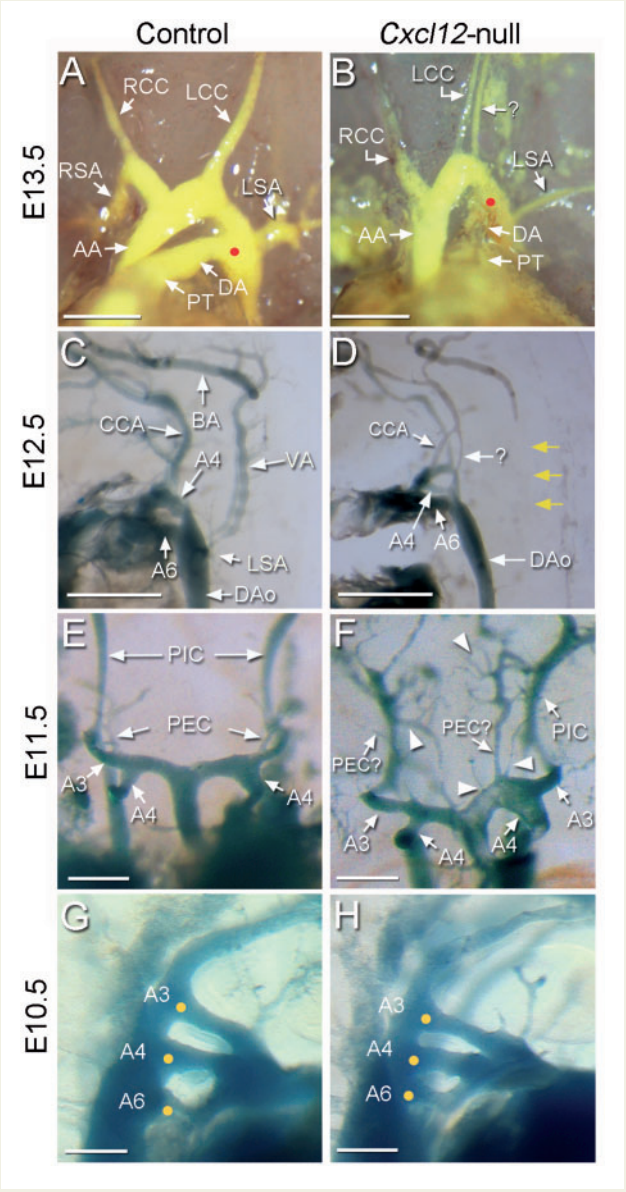

Figure 5 Developmental study of the aortic arch anomaly in *Cxcl12*-null mutants. Developing aortic arch and associated arteries of age-matched control (*A*, *C*, *E*, *G*; $n > 3$ each) and *Cxcl12*-null (*B*, *D*, *F*, *H*; $n > 3$ each) embryos at E13.5 (*A*, *B*), E12.5 (*C*, *D*), E11.5 (*E*, *F*), and E10.5 (*G*, *H*) were compared after visualization with latex dye perfusion. At E13.5, an aberrant arterial branch parallel to LCC, presumed to be LVA is present in *Cxcl12*-mutants (*B*). LSA branches off from the descending aorta (DAo) downstream of the position where the DA intersects with the DAo (red dots) in *Cxcl12*-mutants. In E12.5 embryos, the pharyngeal arches 4 (A4), and 6 (A6) appear to be normal, and the common carotid arteries (CCA) from A3 also develop in *Cxcl12*-mutants. Vertebral arteries that connect subclavian arteries to the basilar artery (BA) (*C*) are absent in *Cxcl12*-mutants (*D*, yellow arrows). Instead aberrant arterial branches are shown (*D*, arrow with question mark). In the AA of E11.5 *Cxcl12*-mutant embryos, numerous aberrant arterial branches are found in AA and AA-associated arteries (*F*, arrowheads). The formation of tree pairs of pharyngeal arches (yellow dots) is largely unaffected in E10.5 *Cxcl12*-mutants (*H*). PIC, primitive internal carotid artery; PEC, primitive external carotid artery. Scale bars: A–D, 500 μm; E–H, 200 μm.

arterial vessels themselves instead of accompanying airways or veins. The branching pattern of arterial vessels was unaffected when *Cxcl12* was deleted in airway epithelial cells by *Nkx2.1*-Cre or *Shh*-Cre (data not shown). These data indicate that pulmonary arterial patterning is not dependent on the chemotactic function of CXCL12 secreted from the most closely associated airway branches. In the development of coronary arteries, CXCL12-deficiency resulted in failure of maturation of coronary arterial system.[8,32] Lack of *Cxcl12* results in disorganization of peritunical plexus and impairs the formation of anastomosis between aortic ECs and the peritunical plexus, and *Cxcl12* in the tunica media of the aorta not in the ventricles is the most critical for this phenotype.[8] It was shown that coronary arteries in the *Cxcl12*-null embryos failed to develop into a higher-order arterial tree.[32] Pulmonary arteries (and also AA arteries) of *Cxcl12*-null mice not only branch off from aberrant positions but also contain extra arterial branches, without affecting the development of venous system. Although there is consistency between coronary and pulmonary arterial development in terms of disorganized arterial vessels, CXCL12 in pulmonary artery development appears to function differently from coronary artery development: there are more pronounced pulmonary arterial branches. Interestingly, deletion of *Cxcl12* from both SMCs (*Tagln*-Cre) and ECs (*Tie2*-Cre) did not affect branching patterns (data not shown). This may suggest that the cellular sources of CXCL12 are more diverse than these two cell types, including perivascular mesenchymal cells. Alternatively, CXCL12 function in arterial patterning is crucial at earlier stages than the timing of its deletion by *Tagln*-Cre and *Tie2*-Cre.

Failure to complete any steps of AA remodelling results in a variety of AA anomalies in human,[33] that have been reproduced in mouse and avian models. Cardiac NCCs contribute to remodelling of the pharyngeal arch arteries (PAA) and septation of the outflow tract.[11] Cardiac NCCs incorporated in PAA differentiate into smooth muscle cells. Defects of cardiac NCCs often impair the regression of the left fourth PAA, and result in an interrupted aortic arch (IAA). The most pronounced phenotype of cardiac NCC defects is persistent truncus arteriosus (PTA), caused by a failure of outflow tract septation. The PTA and/or IAA phenotypes were observed in genetically engineered mouse models of numerous genes involved in the induction, guidance, migration, survival, and differentiation of the cardiac NCC, including *Pdgfra*, *Sema3C*, *Tgfb2*, *Fgf8*, and *Vegfa(164)*.[34–37] HOXA3 and TBX1 have shown to be important for the development of the 3rd and 4th PAA, respectively.[38,39] *Hoxa3*-null mice show an absence of the common carotid arteries.[38] Mice null for *Hey1*, a Notch downstream transcription factor, also exhibited defects in the formation of the 4th PAA, resulting in a right-sided aortic arch (RAA), IAA, and aberrant origin of the right subclavian artery (A-RSA).[40] Endothelin-converting enzyme-1 (*Ece1*)- and the endothelin receptor type A (*Ednra*)-null mice exhibit a right-sided aortic arch and double aortic arches associated with enlargement of the 3rd PAA and the impaired regression of the 4th and 6th PAAs.[41]

Although the AA anomaly and pulmonary artery phenotypes in *Cxcl12*-null mice were in complete penetrance, there may be a variance caused by a mixed strain background. Nonetheless, the AA anomaly phenotype shown in *Cxcl12*-null mice is distinct from the AA anomaly phenotypes associated with the formation and asymmetric regression of PAAs. Studies with avian models have shown that the CXCL12-CXCR4 signalling plays a pivotal role in guidance of cardiac NCCs for the development of PAA.[14–16] Although *Cxcl12*-null mice exhibit ventricular septal defects and occasional outflow malalignment and craniofacial defects, characteristics of *Cxcl12*-null phenotypes in this study do not support essential roles of the CXCL12-CXCR4 signalling in the function of

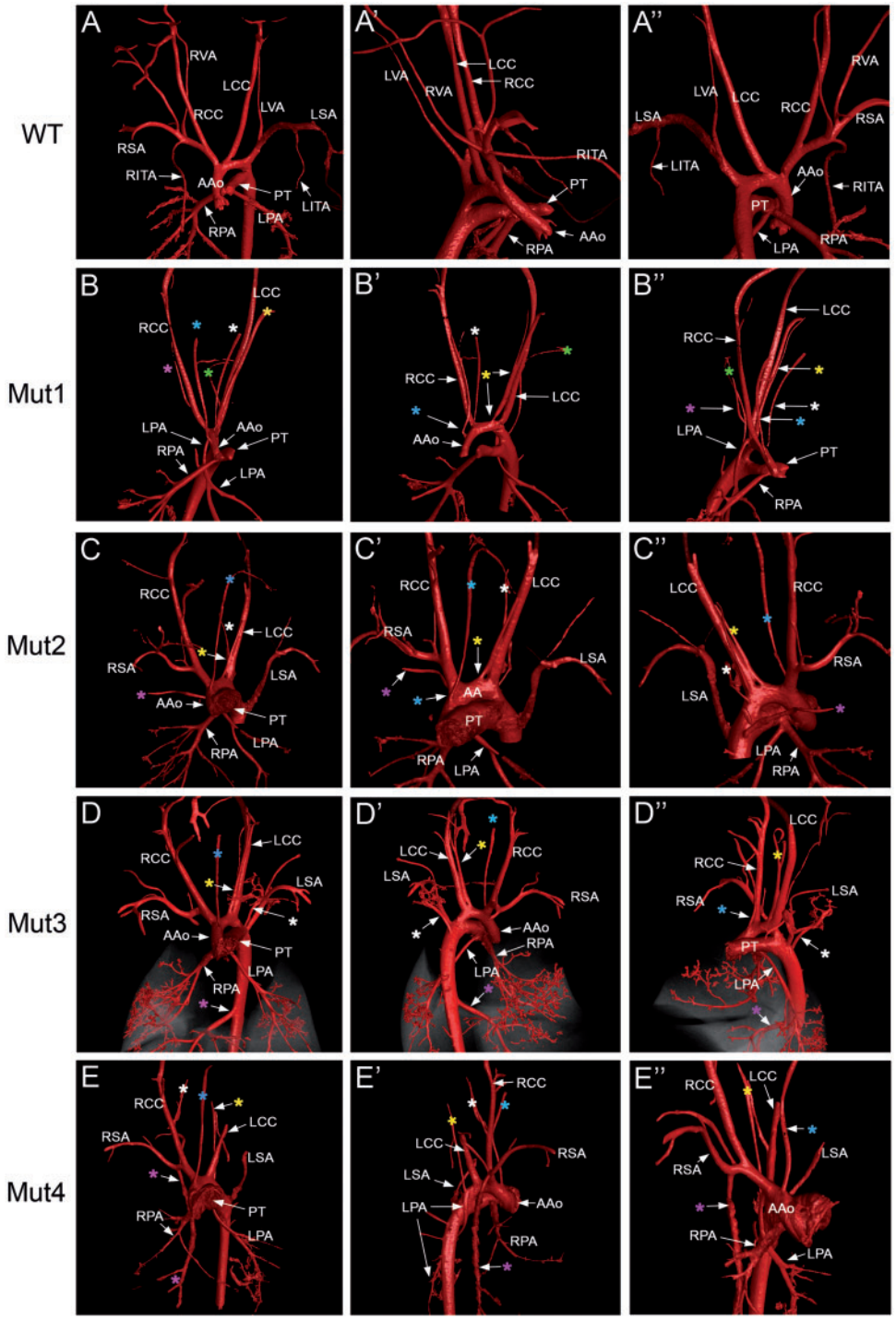

Figure 6 Aortic arch anomaly and abnormal systemic arterial supply to lungs in *Cxcl12*-null mutants revealed by diceCT. AA-associated arteries and pulmonary arteries of E17.5 wild-type (*A*) and four *Cxcl12*-null embryos (*B*–*E*). Images were captured at various angles of 3D images (see Supplementary material online, Video files *S3* and *S4*). The first column shows the frontal view (*A*–*E*), while the second (*A'*–*E'*) and third columns (*A"*–*E"*) show side, oblique, or back views of the same embryo in each row. The colors of the asterisks in each row match to the same aberrant arteries. These AA anomaly phonotypes are essentially the same as those observed by the latex dye perfusion shown in *Figure 4*. Abnormal systemic arterial supplies to the lungs were observed in Mut1 (*B*), Mut3 (*D*), and Mut4 (*E*). LPAs originate from the root of RCC (*B"* and *E"*) or DAo (*D'*), and also RPA from RSA (*E"*).

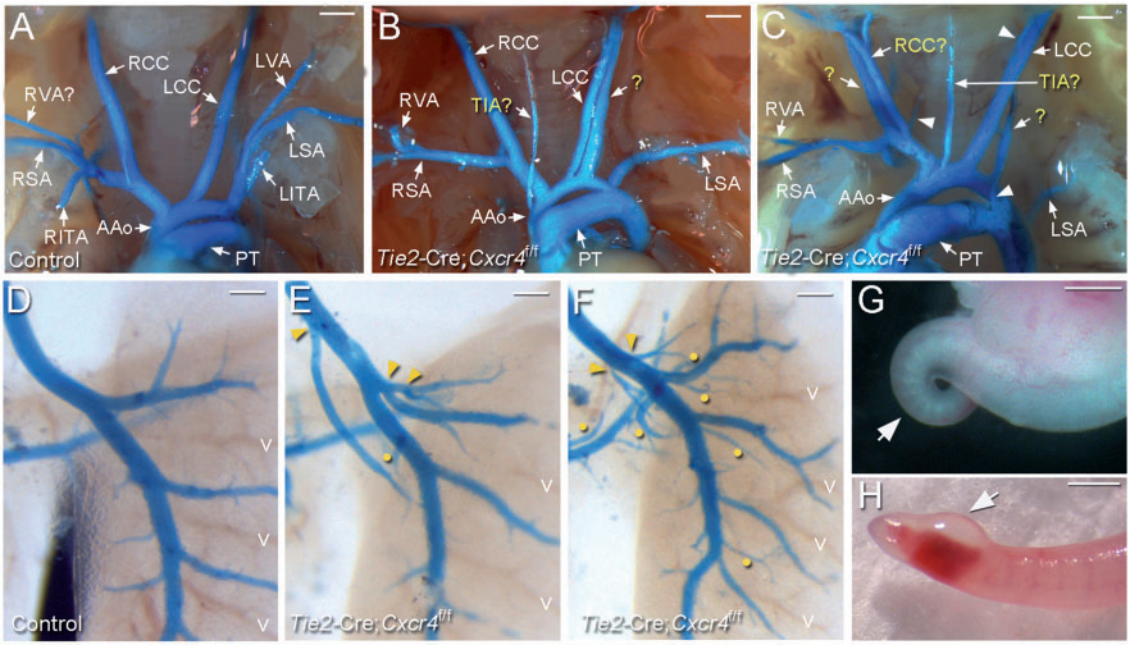

Figure 7 *Tie2*-Cre; *Cxcr4*$^{f/f}$ mice phenocopy *Cxcl12*-null mice. (*A–C*) Ventral view of latex dye-perfused AA arteries of E17.5 control (*A*, $n > 5$) and *Tie2*-Cre; *Cxcr4*$^{f/f}$ (*B*, *C*; $n > 5$) foetuses. Compared to the control, abnormal arteries presumed to be TIA and LVA (marked with '?') are present in the *Cxcr4*-mutants. Additional aberrant arterial branches were found (indicated with arrowheads). LVAs originating from LSA are absent. RITA and LITA: right and left internal thoracic arteries. (*D–F*) Pulmonary arteries of control (*D*, $n > 5$) and *Cxcr4*-mutants (*E*, *F*, $n > 5$) were visualized by the blue latex dye. Aberrant proximal branching points and abnormal superfluous branches in *Cxcr4*-mutants are indicated by arrowheads and yellow dots, respectively. (*G* and *H*) Tail abnormalities in *Cxcr4*-mutant embryos at E12.5 (*G*) and E17.5 (*H*). More than a half of *Cxcr4*-mutants had some forms of tail defect (6/11), including curly, edemic and haemorrhagic tails. Scale bars: A–C and H, 1 mm; D–F, 500 μm; G, 250 μm.

cardiac NCCs for the formation of PAAs. In addition to phenotypic characteristics of *Cxcl12*-null mice, NCC specific deletion of either *Cxcl12* or *Cxcr4* by *Wnt1*-Cre did not affect AA development.

The AA anomaly in *Cxcl12*-null mice is most similar to the vertebral artery (VA) anomaly and abnormal thyroid ima arteries (TIA),[24,25,42,43] which have not been shown by animal models to date. The 7th intersegmental artery extends toward the limbs as the subclavian arteries and elongates cranially as VA which intersect with the basilar artery.[12,44] In VA anomalies, the VAs originates from abnormal positions of the aortic arch. Between LCC and LSA is the most common origin of VA anomalies, but numerous unusual origins have also been reported.[24,42,43,45] TIA is an aberrant artery to the inferior aspect of the thyroid gland, and also has various origins, including brachiocephalic trunk, internal thoracic artery, RSA, and AA.[25] The VA and TIA anomalies by themselves are mostly asymptomatic, but these are critical risk factors for surgeries around the neck and thyroid.[46] The processes by which these congenital anomalies arise have yet to be uncovered. In *Cxcl12*-null mice, we often found an artery parallel to LCC in the absence of VA from LSA and RSA. Based on our data, it seems to be reasonable to describe this abnormal artery parallel to LCC as an aberrant variant of the VA. Subclavian arteries were consistently found below the normal position where the PT-DA meets the DAo. We postulate that CXCL12-CXCR4 signalling may be involved in the formation of the 7th intersegmental arteries at the proper position from which VAs can arise.

In addition to the VA anomaly, numerous additional arteries arose from random positions of the aortic arch or major artery branches in the *Cxcl12*-null mouse. DiceCT images allowed us to identify abnormal systemic arterial supplies to lungs,[47–49] which are often associated with pulmonary sequestration. Since *Cxcl12*-null mice die at perinatal stages, it is unknown how these abnormal systemic supplies to lung would result at later terms, but our result indicates that disturbed CXCL12 signalling might be involved in this pathological cases. The fact that only a limited set of new arteries arise at a certain step of AA development indicates that there must be a mechanism for preventing unwanted sprouting. Superfluous arteries in *Cxcl12*-null lungs and AA infer a role of CXCL12 in protecting arteries from uncontrolled sprouting during development of the aortic arch. This inhibitory role of CXCL12 in sprouting is somewhat contrary to reports showing the promoting role of CXCL12 in angiogenesis.[50,51] Mechanisms underlying the development of AA patterning by CXCL12-CXCR4 signalling need further investigation.

Supplementary material

Supplementary material is available at *Cardiovascular Research* online.

Acknowledgements

We thank Terada, Santostefano, and Fredette for helpful discussions, and Harfe for *Shh*-Cre mouse line.

Conflict of interest: none declared.

Funding

This research was supported by HL64254 and HL128525 to S.P.O., and Korea Mouse Phenotyping Project (2014M3A9D5A01073528) of the Ministry of Science, ICT and Future Planning (MSIP) through the National Research Foundation (NRF) to Y.J.L., in part by NRF grants funded by the Korea government (MSIP) (2017R1A2B4003322 and 2010-0020879) to Y.J.L.

References

1. Karpova D, Bonig H. Concise Review: CXCR4/CXCL12 Signaling in Immature Hematopoiesis–Lessons From Pharmacological and Genetic Models. *Stem Cells* 2015; **33**:2391–2399.
2. Duda DG, Kozin SV, Kirkpatrick ND, Xu L, Fukumura D, Jain RK. CXCL12 (SDF1alpha)-CXCR4/CXCR7 pathway inhibition: an emerging sensitizer for anticancer therapies? *Clin Cancer Res* 2011;**17**:2074–2080.
3. Nagasawa T, Tachibana K, Kishimoto T. A novel CXC chemokine PBSF/SDF-1 and its receptor CXCR4: their functions in development, hematopoiesis and HIV infection. *Semin Immunol* 1998;**10**:179–185.
4. Liekens S, Schols D, Hatse S. CXCL12-CXCR4 axis in angiogenesis, metastasis and stem cell mobilization. *Curr Pharm Des* 2010;**16**:3903–3920.
5. Nagasawa T, Hirota S, Tachibana K, Takakura N, Nishikawa S, Kitamura Y, Yoshida N, Kikutani H, Kishimoto T. Defects of B-cell lymphopoiesis and bone-marrow myelopoiesis in mice lacking the CXC chemokine PBSF/SDF-1. *Nature* 1996;**382**: 635–638.
6. Tachibana K, Hirota S, Iizasa H, Yoshida H, Kawabata K, Kataoka Y, Kitamura Y, Matsushima K, Yoshida N, Nishikawa S, Kishimoto T, Nagasawa T. The chemokine receptor CXCR4 is essential for vascularization of the gastrointestinal tract. *Nature* 1998;**393**:591–594.
7. Ara T, Tokoyoda K, Okamoto R, Koni PA, Nagasawa T. The role of CXCL12 in the organ-specific process of artery formation. *Blood* 2005;**105**:3155–3161.
8. Ivins S, Chappell J, Vernay B, Suntharalingham J, Martineau A, Mohun TJ, Scambler PJ. The CXCL12/CXCR4 Axis Plays a Critical Role in Coronary Artery Development. *Dev Cell* 2015;**33**:455–468.
9. Li W, Kohara H, Uchida Y, James JM, Soneji K, Cronshaw DG, Zou YR, Nagasawa T, Mukouyama YS. Peripheral nerve-derived CXCL12 and VEGF-A regulate the patterning of arterial vessel branching in developing limb skin. *Dev Cell* 2013;**24**:359–371.
10. Plein A, Fantin A, Ruhrberg C. Neural crest cells in cardiovascular development. *Curr Top Dev Biol* 2015;**111**:183–200.
11. Stoller JZ, Epstein JA. Cardiac neural crest. *Semin Cell Dev Biol* 2005;**16**:704–715.
12. Hiruma T, Nakajima Y, Nakamura H. Development of pharyngeal arch arteries in early mouse embryo. *J Anat* 2002;**201**:15–29.
13. Kau T, Sinzig M, Gasser J, Lesnik G, Rabitsch E, Celedin S, Eicher W, Illiasch H, Hausegger KA. Aortic development and anomalies. *Semin Intervent Radiol* 2007;**24**:141–152.
14. Escot S, Blavet C, Hartle S, Duband JL, Fournier-Thibault C. Misregulation of SDF1-CXCR4 signaling impairs early cardiac neural crest cell migration leading to conotruncal defects. *Circ Res* 2013;**113**:505–516.
15. Duband JL, Escot S, Fournier-Thibault C. SDF1-CXCR4 signaling: a new player involved in DiGeorge/22q11-deletion syndrome. *Rare Dis* 2016;**4**:e1195050.
16. Escot S, Blavet C, Faure E, Zaffran S, Duband JL, Fournier-Thibault C. Disruption of CXCR4 signaling in pharyngeal neural crest cells causes DiGeorge syndrome-like malformations. *Development* 2016;**143**:582–588.
17. Herriges M, Morrisey EE. Lung development: orchestrating the generation and regeneration of a complex organ. *Development* 2014;**141**:502–513.
18. Varner VD, Nelson CM. Cellular and physical mechanisms of branching morphogenesis. *Development* 2014;**141**:2750–2759.
19. Farley FW, Soriano P, Steffen LS, Dymecki SM. Widespread recombinase expression using FLPeR (flipper) mice. *Genesis* 2000;**28**:106–110.
20. Lewandoski M, Meyers EN, Martin GR. Analysis of Fgf8 gene function in vertebrate development. *Cold Spring Harb Symp Quant Biol* 1997;**62**:159–168.
21. Seki T, Yun J, Oh SP. Arterial endothelium-specific activin receptor-like kinase 1 expression suggests its role in arterialization and vascular remodeling. *Circ Res* 2003; **93**:682–689.
22. Yuan S, Schoenwolf GC. Islet-1 marks the early heart rudiments and is asymmetrically expressed during early rotation of the foregut in the chick embryo. *Anat Rec* 2000;**260**:204–207.
23. Cai CL, Liang X, Shi Y, Chu PH, Pfaff SL, Chen J, Evans S. Isl1 identifies a cardiac progenitor population that proliferates prior to differentiation and contributes a majority of cells to the heart. *Dev Cell* 2003;**5**:877–889.
24. Dumfarth J, Chou AS, Ziganshin BA, Bhandari R, Peterss S, Tranquilli M, Mojibian H, Fang H, Rizzo JA, Elefteriades JA. Atypical aortic arch branching variants: a novel marker for thoracic aortic disease. *J Thorac Cardiovasc Surg* 2015;**149**:1586–1592.
25. Pratt GW. The thyroidea ima artery. *J Anat Physiol* 1916;**50**:239–242.
26. Gignac PM, Kley NJ, Clarke JA, Colbert MW, Morhardt AC, Cerio D, Cost IN, Cox PG, Daza JD, Early CM, Echols MS, Henkelman RM, Herdina AN, Holliday CM, Li Z, Mahlow K, Merchant S, Muller J, Orsbon CP, Paluh DJ, Thies ML, Tsai HP, Witmer LM. Diffusible iodine-based contrast-enhanced computed tomography (diceCT): an emerging tool for rapid, high-resolution, 3-D imaging of metazoan soft tissues. *J Anat* 2016;**228**:889–909.
27. Li Z, Ketcham RA, Yan F, Maisano JA, Clarke JA. Comparison and evaluation of the effectiveness of two approaches of diffusible iodine-based contrast-enhanced computed tomography (dicect) for avian cephalic material. *J Exp Zool (Mol Dev Evol)* 2016;**326**:352–362.
28. McGrath KE, Koniski AD, Maltby KM, McGann JK, Palis J. Embryonic expression and function of the chemokine SDF-1 and its receptor, CXCR4. *Dev Biol* 1999;**213**:442–456.
29. Berahovich RD, Zabel BA, Lewen S, Walters MJ, Ebsworth K, Wang Y, Jaen JC, Schall TJ. Endothelial expression of CXCR7 and the regulation of systemic CXCL12 levels. *Immunology* 2014;**141**:111–122.
30. Gerrits H, van Ingen Schenau DS, Bakker NE, van Disseldorp AJ, Strik A, Hermens LS, Koenen TB, Krajnc-Franken MA, Gossen JA. Early postnatal lethality and cardiovascular defects in CXCR7-deficient mice. *Genesis* 2008;**46**:235–245.
31. Yu S, Crawford D, Tsuchihashi T, Behrens TW, Srivastava D. The chemokine receptor CXCR7 functions to regulate cardiac valve remodeling. *Dev Dyn* 2011;**240**:384–393.
32. Cavallero S, Shen H, Yi C, Lien CL, Kumar SR, Sucov HM. CXCL12 signaling is essential for maturation of the ventricular coronary endothelial plexus and establishment of functional coronary circulation. *Dev Cell* 2015;**33**:469–477.
33. Keyte A, Hutson MR. The neural crest in cardiac congenital anomalies. *Differentiation* 2012;**84**:25–40.
34. Richarte AM, Mead HB, Tallquist MD. Cooperation between the PDGF receptors in cardiac neural crest cell migration. *Dev Biol* 2007;**306**:785–796.
35. Feiner L, Webber AL, Brown CB, Lu MM, Jia L, Feinstein P, Mombaerts P, Epstein JA, Raper JA. Targeted disruption of semaphorin 3C leads to persistent truncus arteriosus and aortic arch interruption. *Development* 2001;**128**:3061–3070.
36. Bartram U, Molin DG, Wisse LJ, Mohamad A, Sanford LP, Doetschman T, Speer CP, Poelmann RE, Gittenberger-De Groot AC. Double-outlet right ventricle and overriding tricuspid valve reflect disturbances of looping, myocardialization, endocardial cushion differentiation, and apoptosis in TGF-beta(2)-knockout mice. *Circulation* 2001;**103**:2745–2752.
37. Stalmans I, Lambrechts D, De SF, Jansen S, Wang J, Maity S, Kneer P, von der OM, Swillen A, Maes C, Gewillig M, Molin DG, Hellings P, Boetel T, Haardt M, Compernolle V, Dewerchin M, Plaisance S, Vlietinck R, Emanuel B, Gittenberger-De Groot AC, Scambler P, Morrow B, Driscol DA, Moons L, Esguerra CV, Carmeliet G, Behn-Krappa A, Devriendt K, Collen D, Conway SJ, Carmeliet P. VEGF: a modifier of the del22q11 (DiGeorge) syndrome? *Nat Med* 2003;**9**:173–182.
38. Kameda Y, Watari-Goshima N, Nishimaki T, Chisaka O. Disruption of the Hoxa3 homeobox gene results in anomalies of the carotid artery system and the arterial baroreceptors. *Cell Tissue Res* 2003;**311**:343–352.
39. Lindsay EA, Vitelli F, Su H, Morishima M, Huynh T, Pramparo T, Jurecic V, Ogunrinu G, Sutherland HF, Scambler PJ, Bradley A, Baldini A. Tbx1 haploinsufficieny in the DiGeorge syndrome region causes aortic arch defects in mice. *Nature* 2001;**410**:97–101.
40. Fujita M, Sakabe M, Ioka T, Watanabe Y, Kinugasa-Katayama Y, Tsuchihashi T, Utset MF, Yamagishi H, Nakagawa O. Pharyngeal arch artery defects and lethal malformations of the aortic arch and its branches in mice deficient for the Hrt1/Hey1 transcription factor. *Mech Dev* 2016;**139**:65–73.
41. Yanagisawa H, Hammer RE, Richardson JA, Williams SC, Clouthier DE, Yanagisawa M. Role of Endothelin-1/Endothelin-A receptor-mediated signaling pathway in the aortic arch patterning in mice. *J Clin Invest* 1998;**102**:22–33.
42. Koenigsberg RA, Pereira L, Nair B, McCormick D, Schwartzman R. Unusual vertebral artery origins: examples and related pathology. *Cathet Cardiovasc Intervent* 2003;**59**: 244–250.
43. Yuan SM. Aberrant origin of vertebral artery and its clinical implications. *Braz J Cardiovasc Surg* 2016;**31**:52–59.
44. Ha YS, Cho KH, Abe S, Abe H, Rodriguez-Vazquez JF, Murakami G. Early fetal development of the human vertebral artery especially at and above the occipitovertebral junction. *Surg Radiol Anat* 2013;**35**:765–773.
45. Lemke AJ, Benndorf G, Liebig T, Felix R. Anomalous origin of the right vertebral artery: review of the literature and case report of right vertebral artery origin distal to the left subclavian artery. *AJNR Am J Neuroradiol* 1999;**20**:1318–1321.
46. Ozlugedik S, Ozcan M, Unal A, Yalcin F, Tezer MS. Surgical importance of highly located innominate artery in neck surgery. *Am J Otolaryngol* 2005;**26**:330–332.
47. Agarwal PP, Matzinger FR, Shamji FM, Seely JM, Peterson RA. Computed tomography demonstration of systemic arterial supply to lung without sequestration. *Acta Radiol* 2005;**46**:476–479.
48. Ellis K. Fleischner lecture. Developmental abnormalities in the systemic blood supply to the lungs. *AJR Am J Roentgenol* 1991;**156**:669–679.
49. Bhalla AS, Gupta P, Mukund A, Kumar A, Gupta M. Anomalous systemic artery to a normal lung: a rare cause of hemoptysis in adults. *Oman Med J* 2012;**27**:319–322.
50. Salcedo R, Oppenheim JJ. Role of chemokines in angiogenesis: CXCL12/SDF-1 and CXCR4 interaction, a key regulator of endothelial cell responses. *Microcirculation* 2003;**10**:359–370.
51. Salvucci O, Yao L, Villalba S, Sajewicz A, Pittaluga S, Tosato G. Regulation of endothelial cell branching morphogenesis by endogenous chemokine stromal-derived factor-1. *Blood* 2002;**99**:2703–2711.